



ORIGINAL ARTICLE

Investigating the generation of ferrous sulfide nanoparticles in the produced fluid after acidizing oil wells and its influence on emulsifying stability between oil and water



Dongju Li ^{a,*}, Bingkun Gao ^a, Xiangyu Cui ^b

^a College of Electrical and Information Engineering, Northeast Petroleum University, Daqing 163318, China

^b Shantou Development Planning Institute, Guangdong, Shantou, 515000, China

Received 12 May 2022; accepted 18 September 2022

Available online 22 September 2022

KEYWORDS

Nanoparticles;
Surfactant;
Synergistic emulsification;
Oil well flowback fluid

Abstract Studies show that after acidizing operation of oil wells using the alkali/surfactant/polymer (ASP) flooding technology, the produced fluid is emulsified. Since the produced emulsion is stable, it affects the oil–water separation performance. In order to analyze the generation of stable emulsion in the produced fluid after acidizing an oil well, innovative separation experiments were carried out on real oil wells. During the experiments, solid particles in the middle layer of the emulsifying system in the produced fluid after acidizing ASP flooding were extracted and characterized. The generation of the stable emulsifying system in the produced fluid was studied through stability experiments and molecular dynamics simulations. The results showed that the synergistic effect of ferrous sulfide nanoparticles and surfactants was the fundamental reason for the strong emulsifying stability of the produced liquid after acidizing of the ternary composite system. The generation of ferrous sulfide solid particles mainly included two steps. First, sulfate reducing bacteria in injected water by ASP flooding reacted with sulfate in formation water to form hydrogen sulfide. Then, the hydrogen sulfide reacted with iron metal in oil wells and casing of wellbore to form ferrous sulfide particles. It was found that surfactants are adsorbed on the surface of ferrous sulfide nanoparticles. Subsequently, the control ability of surfactant on oil and water phases in the liquid film was enhanced. The performed analyses demonstrate that the adsorption of solid particles to the oil phase was enhanced, while the free motion of molecules in the oil phase at the liquid film position was weakened. The strength of the interfacial film between oil and water was further increased by

* Corresponding author at: Northeast Petroleum University, 99 Xuefu Street, High Tech Industrial Development Zone, Daqing City, Heilongjiang Province, China.

E-mail addresses: lidongjuwenzhang@163.com (D. Li), gaobk@163.com (B. Gao), foxmp551@163.com (X. Cui).

Peer review under responsibility of King Saud University.



Nomenclature

G_1	is the mass of glass crucible with barium sulfate, g;	$C = 0.4116$	is the conversion coefficient of barium sulfate to sulfate;
G_2	is the mass of glass crucible, g;	V_{water}	is the volume of water phase after separation, ml;
W	is the mass of the sample, g;	V_{total}	is the total volume of the total mixture, ml.

the synergistic effect of ferrous sulfide nanoparticles and surfactant. The present study is expected to provide a guideline for a better understanding of the efficient treatment of produced fluids in ASP flooding.

© 2022 The Author(s). Published by Elsevier B.V. on behalf of King Saud University. This is an open access article under the CC BY-NC-ND license (<http://creativecommons.org/licenses/by-nc-nd/4.0/>).

1. Introduction

With the gradual development of onshore oil fields in China in the past few years, the ternary compound flooding system dominated by alkali-surfactant-polymer (ASP) systems has been gradually adopted in old oilfields (Sui et al., 2020). The ASP flooding system has good oil displacement effects (Sun et al., 2020) but there are also some problems. One of the most challenging issues in the ASP flooding technology is the emulsification and formation blockage of the produced fluid. The scaling problem in formation can be solved by using hydrochloric acid and hydrofluoric acid as acidizing working fluid (Di et al., 2021). The phenomenon of emulsifying in the fluid after acidizing is more serious (Keliang and Bowen, 2019). The surfactants and polymers in the ternary composite system and ferrous sulfide nanoparticles formed after acidizing enhance the emulsification degree of the emulsion. Wang et al. (Wang et al., 2020) used a gas detector to analyze toxic and harmful gasses and studied the formation of hydrogen sulfide and carbon monoxide after oil well fracturing. It was found that sulfate-reducing bacteria interact with sour crude and sulfate ion in the formation water and produce hydrogen sulfide gas. Cao et al. (Cao et al., 2021) studied emulsifying systems with different molecular structures and analyzed the effects of surfactants with different molecular structures on the macroscopic viscosity of the emulsion. An et al. (An et al., 2021) performed molecular dynamics simulations and explored the relationship between the adsorption energy of different surfactants and the stability of the emulsion. It was found that the adsorption energy of surfactant enhances the oil–water interfacial energy but reduces the free motion of crude oil and water molecules near the surfactant molecules, thereby reinforcing the emulsion stability. Bai et al. (Bai et al., 2021) extracted fluorosilicate particles from acidizing flow back fluid and showed that in the presence of fluorosilicate particles, the emulsification between oil and water aggravates the acidizing flowback fluid. Zhang et al. (Zhang et al., 2020) synthesized the cashew phenol surfactant and studied the drainage capacity of the emulsion formed by the cashew phenol surfactant and different types of crude oil were studied. Dévora et al. (Cisneros-Dévora et al., 2019) applied the supramolecular assembly and density functional theories to study the stability of crude oil emulsion and the effects of asphaltene molecular structure and acidity of oil and calcium chloride on the stability of the water–oil emulsion. Meanwhile, a modified model was established to improve the accuracy of the stability theory of emulsion. It was found that the stability of emulsion improves under acidizing. Taylor et al. (Taylor and Chu, 2018) explored the interaction between metal ions and crude oil components and revealed that calcium ions would be adsorbed on the surface of crude oil so chelation structures appear on the surface. This composition creates a stable interfacial film on the surface of crude oil. Recently, the stability of the emulsion system has been investigated via various methods such as the electric separation method, centrifugal separation method, and heating separation method. Table 1.

A review of the literature indicates that numerous investigations have been carried out on the emulsification of crude oil (Li et al., 2020; Nishizawa et al., 2016). However, the composition of the emulsion system in the produced fluid after acidizing and plugging removed by ASP flooding was complex. Meanwhile, there is no in-depth understanding of the emulsification theory of solid particles. Zhang (Qing et al., 2015) used a strong electric field separation method and analyzed the main controlling factors of the emulsification stability of the emulsion system. However, the microscopic interaction between the oil phase, water phase, and solid phase is complicated and the emulsion is not stable (Li et al., 2022; Wei et al., 2015; Barg et al., 2012). Since this complexity mainly originates from solid particles, it is necessary to carry out in-depth investigations on the influence of solid particles on the properties of the produced fluid. Moreover, the main components of solid particles and their synergistic mechanism with surfactants should be analyzed. In order to study the generation and stabilization mechanism of emulsion in the produced fluid after acidizing oil wells of ASP flooding, the research flowchart is shown in Fig. 1.

To this end, the produced fluid after acidizing oil wells of ASP flooding was selected and a strong stable emulsion of the middle layer was obtained by centrifugal separation experiment. To remove the oil phase, the separated emulsion was cleaned with acetone and petroleum ether so the oil and water phases were separated. The solid particles in the middle layer of the emulsion were separated by filtration and drying. The chemical composition of solid particles were analyzed using scanning electron microscopy (SEM) and an X-ray diffractometer. Then the ionic components in the aqueous phase of the produced liquid were analyzed and the sulfate content was measured. The culture experiment of sulfate-reducing bacteria was conducted to determine whether the produced liquid contains sulfate-reducing bacteria. Through a high-temperature and high-pressure reaction kettle combined with a bacterial culture experiment, the reaction of metabolites of sulfate-reducing bacteria with iron particles in the stratum and the production of ferrous sulfide particles were analyzed. Then the size distribution of the produced ferrous sulfide particles was measured using a laser particle size analyzer. Finally, emulsification experiments, microscopic observation experiments, emulsion stability experiments under the action of the electric field, and the obtained results from molecular dynamics simulation were combined to analyze the generation of strong stable emulsion in the produced fluid after acidizing oil wells of ASP flooding. The synergistic characteristics of solid particles, oil, water, and surfactant in the emulsion liquid film were analyzed according to the root mean square (RMS) displacement and density distribution function as indices. This article is expected to provide a guideline to better understand the generation mechanism of strong stable emulsion systems in the produced fluid after acidizing oil wells of ASP flooding, which is of great significance to the efficient treatment and environmental protection of produced fluid in oilfields.

Test bottle with bacterial growth	1	2	3	4	5
Number of bacteria(pcs/mL)	1–10	10–100	100–1000	1000–10000	10000–100000

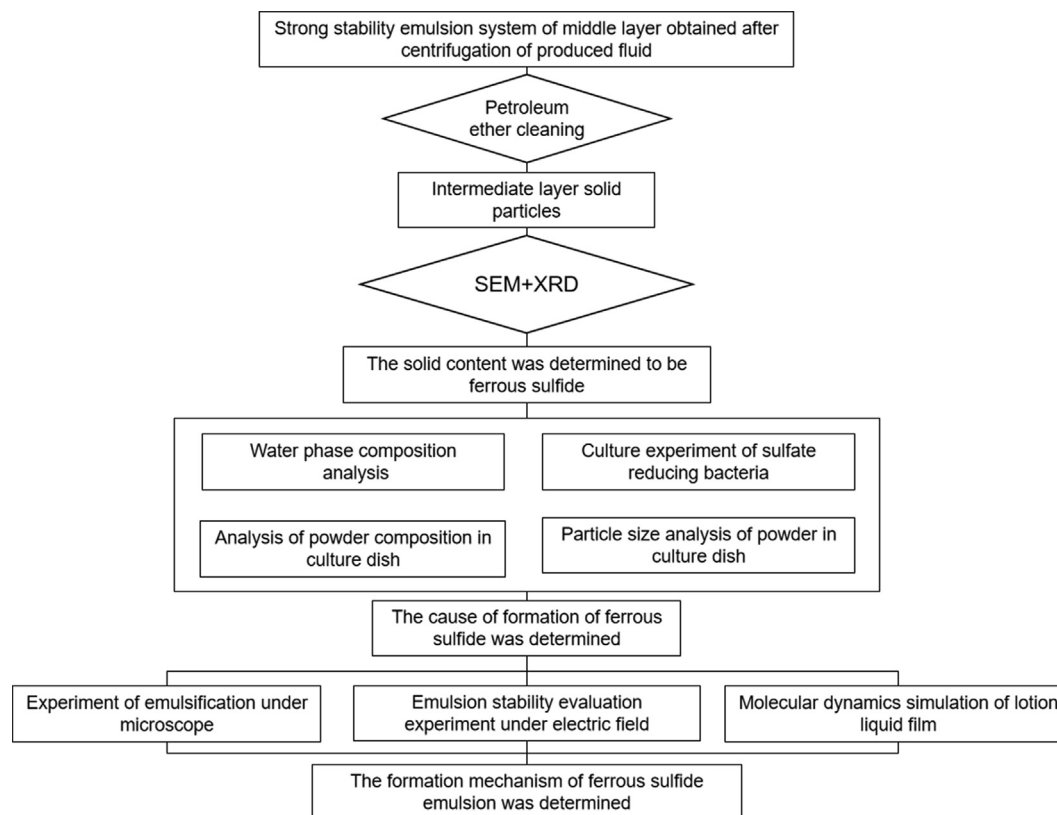


Fig. 1 Research flowchart.

2. Experiments and simulations

2.1. Experimental part

2.1.1. Experimental materials and equipment

Crude oil, Produced fluid after acidizing of ASP flooding and rock powder were prepared from Oil Production Plant No.1 of Daqing Oilfield. OP-10 (analytically pure) and sodium dodecyl sulfate (analytically pure) were provided by Dongguan Xunye Chemical Reagent limited company. Pure sodium dodecyl benzene sulfonate and Petroleum ether were prepared from Guangzhou Jiangshun Chemical Technology limited company and Hefei Henggong Environmental Technology limited company, respectively. Moreover, the RSB-HX-7 sulfate-reducing bacteria test bottle was prepared by Shanghai Biaozhuo Scientific Instrument limited company. It is worth noting that pure sodium hydroxide, pure ferrous chloride, pure ferric chloride, pure acetone, and pure sodium sulfate were used in the experiments. Centrifuge, SEM, and X-ray diffractometer were used to extract and characterize solid particles in the middle layer of

the produced liquid. A 100 mL beaker, a 1 mL syringe, and an electro-thermal incubator were used to detect sulfate-reducing bacteria in water samples. A high-temperature high-pressure reactor and a gas detector (Company ADKS-4, Country) were used in the experiments.

2.1.2. Experimental principles

(1) Extraction and characterization of solid particles in the middle layer of the extraction liquid:

The produced fluid after acidizing ASP flooding was poured into a 50 mL centrifuge tube. Then the tube was centrifuged at 3000 r/min for 10 min. The produced liquid after centrifuging was divided into three separate layers. The middle layer was extracted by removing the upper oil layer and the lower water layer using an injector. The middle layer was initially cleaned using petroleum ether and acetone to remove the oil phase. Then the mixture was dried at 70 °C to remove the water phase and extract solid particles. The structure, size, and composition of solid particles in the middle layer were observed by SEM and X-ray diffractometer.

(2) Investigating the generation mechanism of ferrous sulfide nanoparticles in the produced fluid after acidizing oil wells.

Detection of ionic components in the water sample

The water sample was filtered to remove the floating components and solid particles. Moreover, the organic components were removed by injecting hydrogen peroxide into the flow. Then the sample was dried to a constant weight and the mineralization degree of the water sample was calculated.

Hydrochloric acid was added to the sample solution to reach a weakly acidic solution. The barium sulfate precipitation was formed by adding barium chloride solution to the prepared acidic solution. In order to calculate the content of sulfate, barium sulfate precipitation was filtered, washed, and dried to a predefined weight in the glass crucible. The sulfate content can be calculated as follows:

$$\text{Sulfate radical}(\%) = \frac{(G_1 - G_2)}{W} \times 0.4116 \times 100 \quad (1)$$

Where G_1 , G_2 , and W denote the weight of the glass crucible and barium sulfate, glass crucible, and sample, respectively. The coefficient 0.4116 is the conversion coefficient of barium sulfate to sulfate.

Detection of sulfate-reducing bacteria in water samples

The content of sulfate-reducing bacteria in the water sample was determined using the extinction dilution method, in which the sample was taken out with sterile syringes and injected into test bottles for stepwise dilution. Each test bottle diluted the number of bacteria in the water by 10 times. The test bottles were placed in an electro-thermal incubator with a constant temperature of 35 °C. After seven days of culture, the change of the test bottles was recorded. The bacterial content in each group of injected water samples was recorded according to the following bacterial count table.

Investigating the formation of ferrous sulfide particles based on sulfate-reducing bacteria

In order to determine whether ferrous sulfide particles produce by sulfate-reducing bacteria, an experimental device was

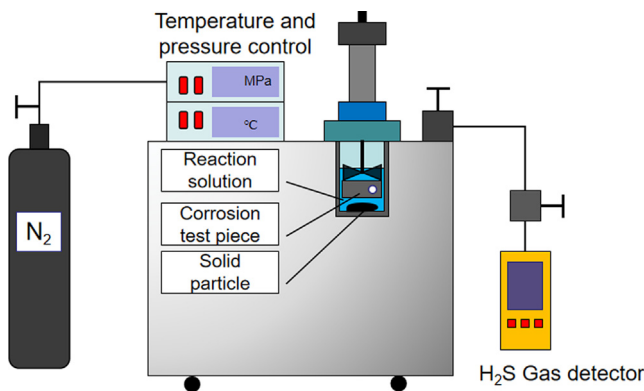


Fig. 2 Schematic of ferrous sulfide particle generation equipment based on sulfate-reducing bacteria.

designed as shown in Fig. 2. The 50 mL produced fluid containing sulfate-reducing bacteria after acidizing the oil well was filtered to remove floating oil and solid particles. Then the mixture was put in a high-temperature high-pressure reactor. Moreover, 50 mL sodium sulfate solution of 2 % mass concentration and iron corrosion test piece were placed in the high-temperature high-pressure reactor. During the experiments, temperature and pressure were set to 35 °C and 5 MPa. To this end, a temperature–pressure controller shown in Fig. 1 was used. After 24 h, 48 h, 72 h, 96 h, and 120 h, the control valve was opened and the reaction gas was collected with a gas collection bag. The hydrogen sulfide content in the reactor was measured using a gas detector (Model ADKS-4, Country). When the pressure relief was completed, the iron corrosion test piece was taken out and its corrosion degree was measured. Meanwhile, solid particles on the surface of the iron test piece and in the solution were extracted. Then the extracted particles were dried to analyze the composition of minerals and determine whether ferrous sulfide particles are produced.

(3) Emulsion stability evaluation.

The mixed solution of 50 mL crude oil and 50 mL distilled water was placed in a homogenizer and stirred at 30,000 r/min for 5 min. The emulsifying results were observed by microscope. Then the mixed solution was placed into the demulsifier selector with a high voltage electric field of 4.5 kV at an ambient temperature of 90 °C. After 5 min, the stratification performance of oil and water was analyzed and the volume fraction of the water phase in the mixed solution was calculated. Fig. 3 shows the demulsifier selector and the separation mechanism.

It should be indicated that under the influence of the oil phase and the mixing of emulsion, the volume of the emulsion cannot be identified. Accordingly, only the water phase volume could be measured and there is no obvious correlation between the oil phase volume and the water phase volume in the emulsion under different conditions. Consequently, the emulsion stability was evaluated by calculating the percentage of water phase volume to the total volume of the mixture under different conditions. This can be mathematically expressed as follows:

$$S = \frac{V_{\text{Water}}}{V_{\text{Total}}} \times 100\% \quad (2)$$

In this section, it is intended to investigate the influence of different surfactants and solid particles on the stability of emulsions. To this end, distilled water in the system was changed to 0.2 % of the surfactant solution, and 0.5 g of solid powder was added to the mixture to carry out emulsification experiments under the same conditions. Finally, the emulsification results were monitored.

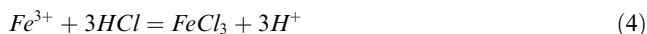
(4) Experimental mechanism of synergistic effect between solid particles and surfactant:

To investigate the mechanism of synergistic effect between solid particles and surfactant in the produced fluid after acidizing of ASP flooding, the performance of silica nanoparticles, calcium carbonate nanoparticles, and ferric sulfide nanoparticles was analyzed and compared. Then the reaction products were analyzed. During the acidizing process, the metals in ground pipelines reacted with acid liquor and ferrous chloride and ferric chloride are produced. These reactions are as follows (Hong, 2012):





Fig. 3 Demulsifier selector and its electrical separation mechanism.



There was a certain amount of sodium hydroxide in the ternary system. Under the action of alkali, iron hydroxide and colloidal ferrous hydroxide are produced in reactions (3) and (4). Moreover, the variation of pH was unstable during the acidizing process of ASP flooding. In the presence of sulfur in formation fluids, ferric sulfide and ferrous sulfide are likely to be produced (Wang et al., 2020).

Based on the foregoing reaction principles, emulsifying stability under different types of iron metal conditions was analyzed. To analyze the reaction (3), 0.2 g ferric chloride and 0.2 g ferrous chloride were initially added to the oil–water emulsion, and then sodium hydroxide was added.

2.2. Theoretical analyses

In order to clarify the influence of iron sulfide nanoparticles on the stability of crude oil emulsion, the influence of iron sulfide and ferrous sulfide on the free movement of surfactant molecules and crude oil molecules was studied. The interfacial adsorption energy between oil molecules and water molecules under different conditions was calculated using LAMMPS molecular dynamics simulator. To simplify the calculations, the crude oil was considered C5 (Huang et al., 2021; Bin et al., 2022). The total number of xxx was set to 100 and water molecules were simulated using the TIP4P model. Then the surfactant molecules were placed between crude oil molecules and water molecules. It should be indicated that 100 water molecules and 20 surfactant molecules were used in the calculations. Moreover, 10 iron sulfide molecules were added to the surfactant phase. The initial model was obtained by minimization operation as shown in Fig. 4.

Fig. 4a, 4b, and 4c show molecules of crude oil, surfactant, and water, respectively. These three molecules were placed in a unified crystal to simulate the distribution of oil, surfactant, and water molecules in the liquid film. It should be indicated that the surfactant is between the oil phase molecules and the water phase molecules. The Lennard-Jones potential model with a truncation radius of 12.5 Å was used to simulate the intermolecular interaction between molecules (Cao et al., 2021). Moreover, the long-range Coulomb force was calculated using the particle–particle particle-mesh (PPPM) algorithm. After constructing the initial model, the vibration of the crude oil component near its geometric position was modeled using the Shake method, in which each component was fixed at a certain position. The system was simulated in NVT ensemble for 2 ns and the simulation step was set to 0.01 ps.

A Nose-Hoover thermostat was used to keep the temperature of the system at 293.15 K.

Based on this model, the dynamic characteristics and density distribution of water molecules before and after adding surfactants and ferric sulfide particles were studied. Meanwhile, the synergistic mechanism between iron sulfide nanoparticles and surfactants was analyzed.

3. Results and analysis

3.1. Identification and characterization of intermediate solid particles in the emulsification system

In the previous sections, the oil phase in the produced fluid after acidizing of ASP flooding was separated by centrifuge and the middle layer was analyzed by a microscope. Then the mixture of the middle layer was treated with petroleum ether and acetone, and dried in the oven. Fig. 5 shows the olive brown powder obtained from the SEM.

Fig. 5 shows that after centrifugal separation treatment, there is a distinct intermediate layer of material in the middle of the oil phase and the water phase, which was neither the transparent water phase nor the black oil phase, but a grayish-brown material in between. Separating the mixture in the middle layer revealed that there are more oil-phase substances in the middle layer. Moreover, the microscopic images in Fig. 5b demonstrate that the emulsification system mainly consists of water–oil emulsion. Since the density of the emulsion was between the oil phase and the water phase, an intermediate layer was formed at the interface of the two phases. Similarly, it is inferred that the density of solid particles in the middle layer was between the density of the oil phase and the density of the water phase. Accordingly, the intermediate emulsification system remains stable even under strong centrifugal forces so it exists between the oil and water phases. The SEM images reveal that the morphology and geometry of nanoparticles are very complex and irregular. Moreover, the surfaces of nanoparticles are uneven and very rough. The size of nanoparticles was distributed in a wide range, which included large particles of several microns to small particles of a few hundred nanometers. The vast majority of particles were small particles less than one micron in diameter.

The element composition analysis was carried out using energy dispersive X-ray spectroscopy (EDX) at different positions.

The selected sample areas and element composition are shown in Fig. 6 and Table 2, respectively. It is found that

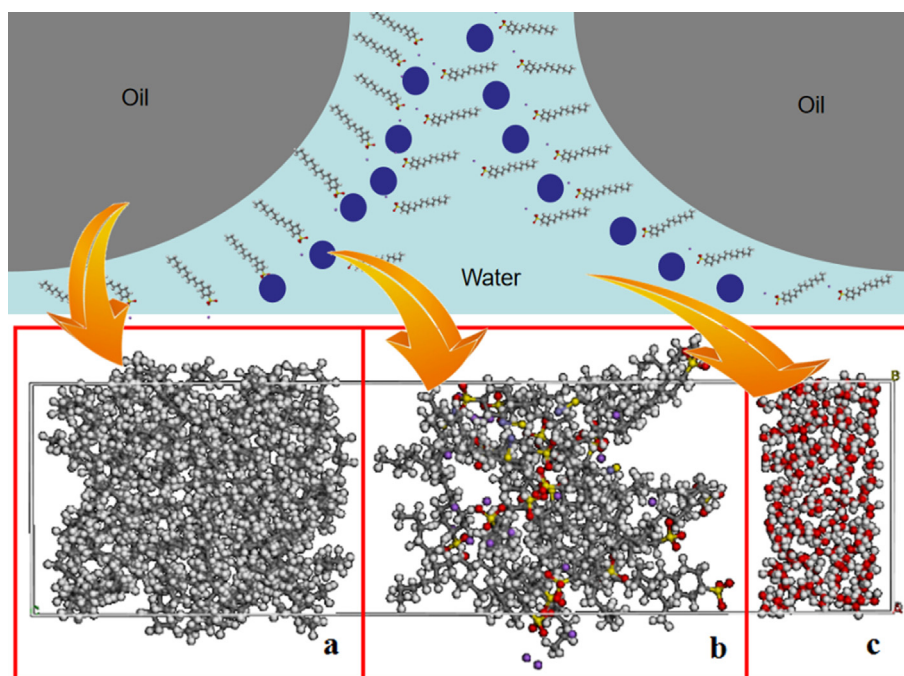


Fig. 4 Crude oil model: (a) surfactant molecules, (b) solid iron sulfide molecules, and (c) water molecules.

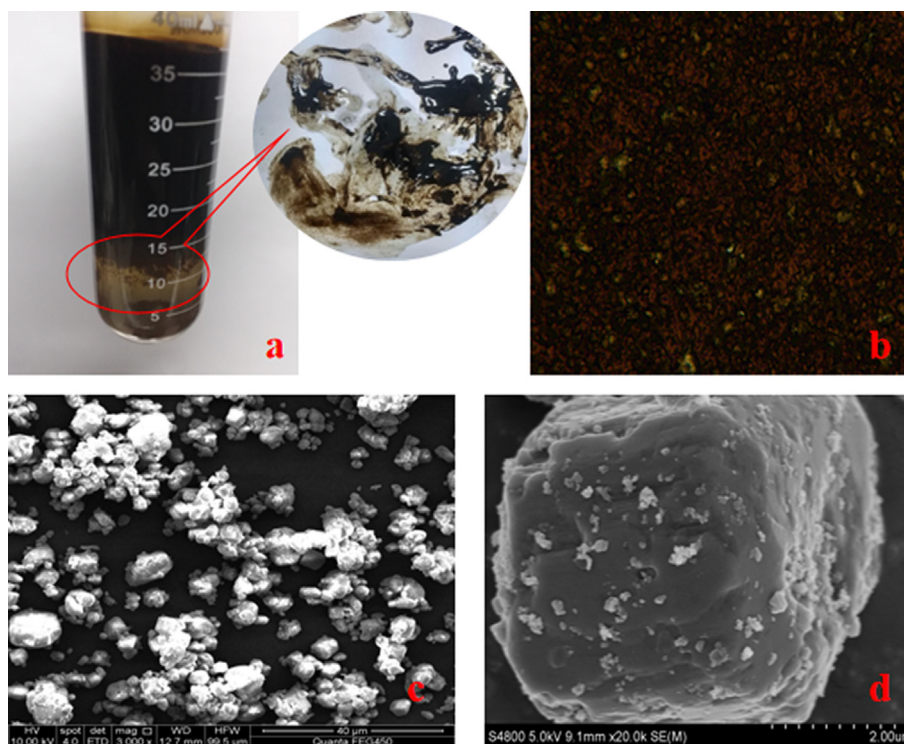


Fig. 5 SEM images of the solid nanoparticles on the electrode plate a. Intermediate layer material after centrifugation of the produced liquid; b. The intermediate layer material under a microscope; c. Solid particles after separation of the intermediate layer material; d. SEM of solid particles.

the sample areas mainly consist of Ca, C, O, Si, S, and Fe elements, and the sum of mass fraction of these six elements are 84.98 % and 95.52 %, respectively. It is concluded that these elements are the main components of solid nanoparticles in crude oil. The sample areas in Fig. 6b contained Ca, C, O,

Si, S, Fe, and Ba elements with a mass fraction sum of 97.08 % and 97.25 %, respectively. It should be indicated that solid nanoparticles also contained some trace elements such as Ba, Na, Al, Mg, Mn, and Ti, which may originate from clay particles and metal minerals in the formation.

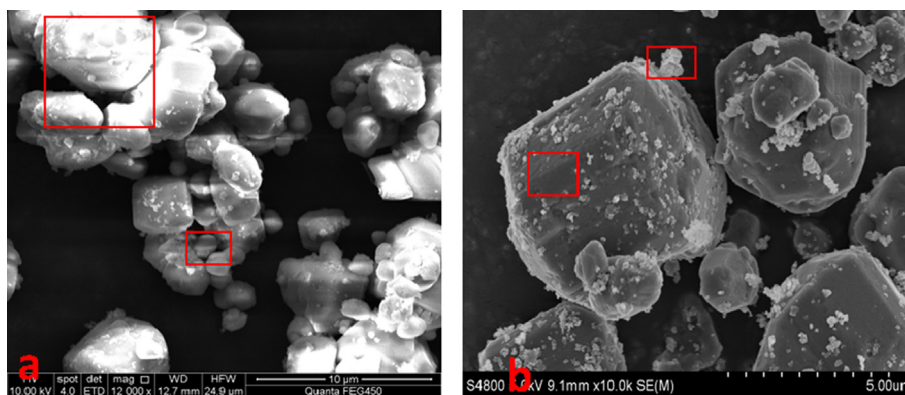


Fig. 6 SEM images and sample area of element composition of solid particles in the middle layer after separation.

Table 2 The composition of solid nanoparticles in the middle layer.

Element	Mass fraction of different elements			
	Sample areas 1	Sample areas 2	Sample areas 3	Sample areas 4
C	48.81	19.31	28.85	10.89
N	13.62	–	–	–
O	32.73	40.99	42.59	33.04
Na	0.33	–	0.56	0.65
Mg	0.19	2.3	0.46	–
Al	0.88	0.58	1.57	0.5986
Si	1.9	1.7	4.98	0.7058
S	0.28	–	1.54	9.01
K	–	–	0.34	–
Ca	0.35	0.41	1.73	–
Fe	0.91	33.11	12.7	3.54
Mn	–	1.59	–	–
Ba	–	–	4.69	39.87

The elements of the separated solid nanoparticles were also analyzed by EDX. The obtained results show that the adsorbed solid particles contain Ca, C, O, Si, S, Fe, and Ba elements mainly in the form of SiO_2 , CaCO_3 , FeCO_3 , $\text{Fe}_{(1-x)}\text{S}$, and BaSO_4 , which are the main products of the oilfield scaling. Generally, SiO_2 is released by the dissolved aluminum silicate of alkaline substances in the ASP flooding, while CaCO_3 is produced when the dissolution equilibrium of carbonate breaks. Moreover, $\text{Fe}_{(1-x)}\text{S}$ and FeCO_3 are produced in complex chemical reactions in sulfate-reducing and iron bacteria on corroded particles of crude oil gathering and transportation equipment. BaSO_4 mainly forms by the dissolution of drilling mud and incompatibility between the injected water and the formation water. The constituent element ratio of iron sulfides was neither 1:1 nor 1:2, indicating that iron sulfides were probably a mixture of different compositions. The iron sulfide was dissolved to analyze its ionic elements, and it was found that the valence state of Fe was + 2, and S was the mixed valence state of –1 and –2. The results of element analysis in [Table 3](#) indicate that $\text{Fe}_{(1-x)}\text{S}$ composition mainly consists of $\text{Fe}_{(0.8)}\text{S}$ and FeS.

3.2. Generation mechanism of ferrous sulfide nanoparticles in the produced fluid after acidizing oil wells

In this section, the mineralization degree, sulfate content, chloride ion content, and sulfate-reducing bacteria content of the

Table 3 The results of $\text{Fe}_{(1-x)}\text{S}$ composition analysis.

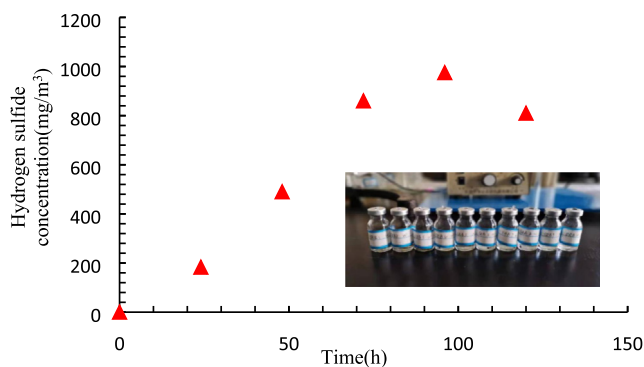
Elemental composition of $\text{Fe}_{(1-x)}\text{S}$	Fe (ppm)	S (ppm)	Molecular formula
1	2.519	1.527	$\text{Fe}_{(0.8)}\text{S}$
2	1.034	0.623	FeS

produced fluid after acidizing oil wells of ASP flooding were measured based on the discussed experimental process in section 2.1. The obtained results are presented in [Table 4](#).

[Table 4](#) reveals that the mineralization degree of the produced liquid is 4514.65 mg/L, which is relatively high. The produced liquid contained sulfate, which could provide a sufficient sulfur source for sulfate-reducing bacteria. During the experiment, small iron nails in the SRB-HX-7 sulfate-reducing bacteria test bottle become black. Meanwhile, the culture medium in the bottle becomes turbid, and black aggregates precipitate. This phenomenon reflects the existence of sulfate-reducing bacteria in the produced liquid. Further investigations ([Mahdavi et al., 2017](#); [Sharma et al., 2015](#)) show that sulfate-reducing bacteria could restore sulfate ions in water so hydrogen sulfide gas is produced in the formation. Then iron in the acidic environment of the wellbore reacts with hydrogen sulfide and ferrous sulfide particles are produced. This reaction can be expressed as follows:

Table 4 Test results of the samples in the produced liquid after acidizing of ASP flooding.

Testing items	Mineralization degree(mg/L)	Sulfate(mg/L)	Chloride ion(mg/L)	Sulfate reducing bacteria(ppm/ml)
Test results	4514.65	44.95	1095.16	1000–10000

**Fig. 7** The distribution of the hydrogen sulfide concentration in the reactor.

The generation of ferrous sulfide particles originating from sulfate-reducing bacteria was studied to analyze the formation mechanism of these particles in the produced fluid after acidizing oil wells of ASP flooding. The hydrogen sulfide content in the reactor was measured using the gas detector.

The obtained results in Fig. 7 reveal that as the reaction time increases, the hydrogen sulfide content in the reactor increases first and then decreases. This trend may be attributed to a large number of sulfate-reducing bacteria in the produced fluid of acidizing oil wells after ASP flooding, which react with sulfate and produce hydrogen sulfide gas. However, when the concentration of hydrogen sulfide gas in the reactor increases, it reacts with metal in the formation wellbore, thereby decreasing the hydrogen sulfide content in the wellbore environment.

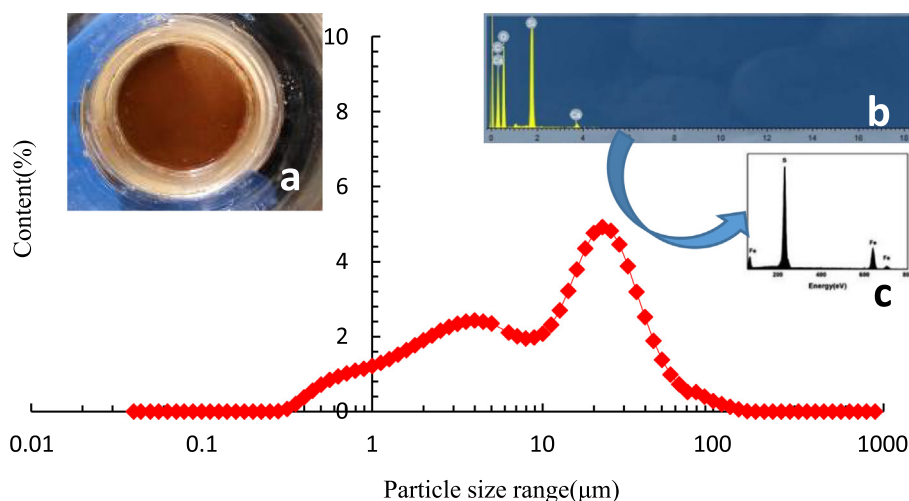
The iron corrosion test piece in the reactor was taken out and the solid powder on the surface of the test piece was

scraped. The solution in the reactor was filtered to obtain the olive brown powder. Then the morphology and size distribution of particles were measured by SEM, and the chemical composition was analyzed by energy dispersive spectrometer (EDS).

Fig. 8 indicates that the size range of solid particles in the reactor was wide and varied from 0.35 μm to 141 μm . It is found that the smallest particles are of nanoscale. The wide difference in the size of solid particles may originate from the following two factors: On the one hand, large particles would be produced by the reaction between hydrogen sulfide and iron in the reactor. On the other hand, corroded iron particles may be oxidized so Fe_2O_3 is produced. Fig. 8b shows that Ca and Si elements exist in solid particles. This phenomenon could be interpreted by the low pH of the produced fluid after acidizing oil wells of the ASP flooding so calcium silicate particles dissolve in the produced fluid, and silicon and calcium ions are produced. After adding a certain amount of sodium sulfate solution into the reactor, the pH of the fluid increases, and a part of calcium silicate particles precipitate. Solid particles contain large amounts of O and Fe elements indicating that iron might be oxidized to ferric oxide, which is consistent with the previous analysis. Fig. 7c reveals that solid particles contain S and two types of Fe elements simultaneously. Therefore, in addition to calcium silicate and ferric oxide, ferrous sulfide particles were also produced in the reactor.

3.3. The influence of synergistic effects of surfactant and solid nanoparticles on the emulsifying capacity

In order to compare the emulsifying effect of the produced fluid before and after acidizing to remove the skin damage of wells by ASP flooding, it is necessary to analyze the

**Fig. 8** The composition and size distribution of solid particles in the reactor.

microstructures and microscopic images. The emulsifying effects of the produced fluid under different conditions are presented in Fig. 9.

The analysis of the microscopic images of the produced liquid demonstrates that the properties of oil–water emulsions change significantly under different conditions. The comparison of Fig. 9A, 9B, and 9C reveal that there is no emulsification after mixing with oil and water. When the water phase is replaced by the clear supernatant of the produced liquid, sporadic water drops remain in the emulsifying system, which significantly increases the emulsification degree. After adding solid particles, the emulsification degree of the whole system increased significantly and a stable water–oil emulsion system was formed. This phenomenon indicates that for the emulsifying system of the produced fluid after acidizing of the ASP flooding, the polymer and surfactant in the water phase do not affect the emulsification degree of the whole system, while enhancement of the emulsification degree of the system mainly originates from solid particles. After adding ferric chloride, ferrous chloride, and sodium hydroxide into the system, colloidal ferric hydroxide and colloidal ferrous hydroxide are produced. Fig. 9D – 9F indicate that although colloidal ferric and

ferrous hydroxide are produced, the emulsification degree of the system is still less than that of Fig. 9C. Fig. 9F shows that pure solid particles do not complicate the emulsification degree. The comparison of Fig. 9G, 9H, and 9I reveal that the emulsification degree of the system increases obviously under the synergistic effect of surfactant and solid particles, which is consistent with the trend shown in Fig. 9C. Accordingly, it is concluded that the strong emulsifying stability of the produced liquid after acidizing of the ASP flooding mainly originates from the synergistic effect of ferrous sulfide nanoparticles and surfactants.

There is no clear correlation between the emulsification degree and the emulsifying stability. Therefore, nine emulsion formulation systems in Fig. 8 were selected in the stability experiments to verify the abovementioned theories. At high-temperature and high electric field strength, the stability evaluation experiment was carried out according to the method discussed in section 2.1. The obtained results in this regard are presented in Table 5.

Table 5 indicates that the maximum electric field strength that can be applied to emulsions under different emulsifying systems was also different. In some systems, it is not possible

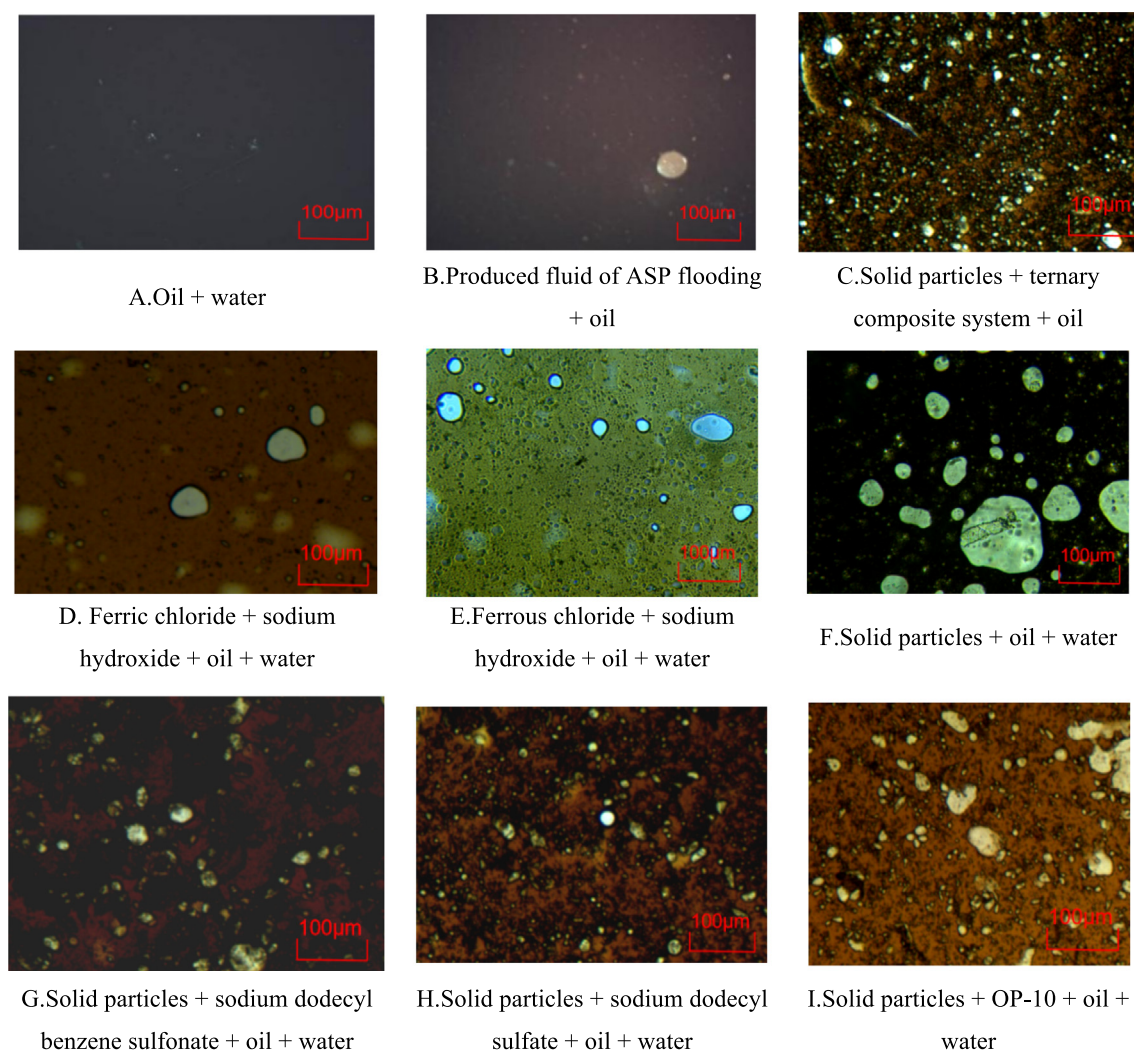


Fig. 9 Microscopic images of the emulsifying system under different conditions.

to separate oil–water emulsion even at high temperatures and high electric field strengths. The comparison of different conditions demonstrates that oil–water separation could be achieved in the emulsion systems A (oil + water), B (produced fluid of ASP flooding + oil), D (ferric chloride + sodium hydroxide + oil + water), E (ferrous chloride + sodium hydroxide + oil + water), and F (solid particles + oil + water). In other words, it is not possible to separate oil–water emulsion in the emulsion systems C (solid particles + ternary system + oil), G (solid particles + sodium dodecyl benzene sulfonate + oil + water), H (solid particles + sodium dodecyl sulfate + oil + water), and I (solid particles + OP-10 + oil + water). These results verify that the strong stability of emulsion after acidizing of the ASP flooding mainly originates from the synergistic effect of ferric nanosulfides and surfactant.

3.4. Investigating the synergistic mechanism of the surfactant and solid nanoparticles

In this section, the synergistic mechanism between the surfactant and solid nanoparticles was analyzed based on the discussions raised in Section 3.3. To this end, the influence of surfactant and ferric sulfide nanoparticles in the emulsion on the density distribution and free movement ability of water molecules were analyzed by molecular dynamics simulations. The density distributions of oil, water, and surfactant molecules under different conditions were simulated and the obtained results are shown in Fig. 10.

Fig. 10 shows that when the surfactant was added, it forms an interface emulsion film in the middle of the oil phase and the water phase, which covers the interface between the two

Table 5 The results of the emulsion stability under different conditions.

Item	Stability of emulsion system								
	A	B	C	D	E	F	G	H	I
Stability (%)	50.00	49.20	21.18	48.96	47.52	47.31	30.25	29.23	27.14
Maximum voltage that can be applied (kv)	4.25	4.25	1.21	4.25	4.25	4.25	1.68	1.54	1.14
Whether can be demulsification	Yes	Yes	No	Yes	Yes	Yes	No	No	No

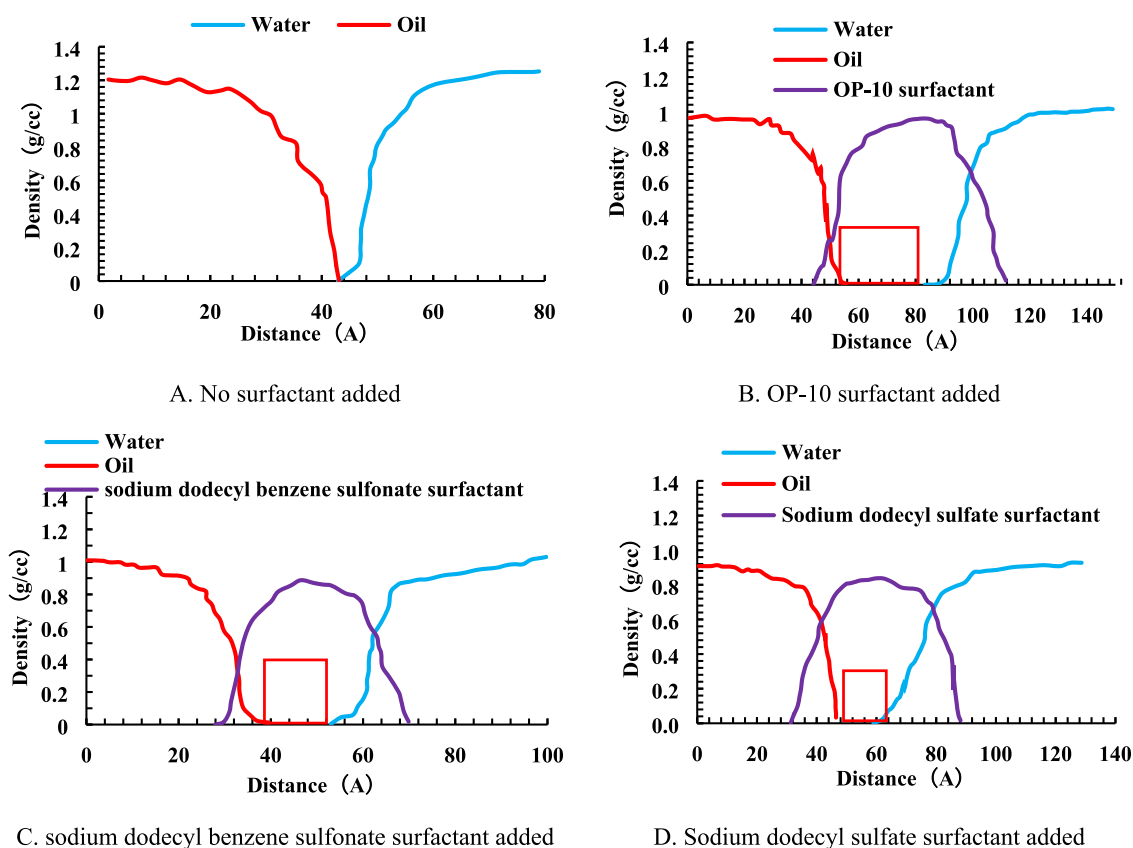


Fig. 10 Distribution of oil, water, and surfactant at the interface film of emulsion under different conditions.

Table 6 The results of the interfacial distance between water and oil molecules and the stability of the emulsion.

Comparison content	Oil + water	Solid particles + sodium dodecyl benzene sulfonate + oil + water	Solid particles + sodium dodecyl sulfate + oil + water	Solid particles + OP-10 + oil + water
Interfacial distance (A)	0	17	12	42
Stability (%)	50	30.25	29.23	27.14
Maximum voltage that can be applied (kv)	4.25	1.68	1.54	1.14

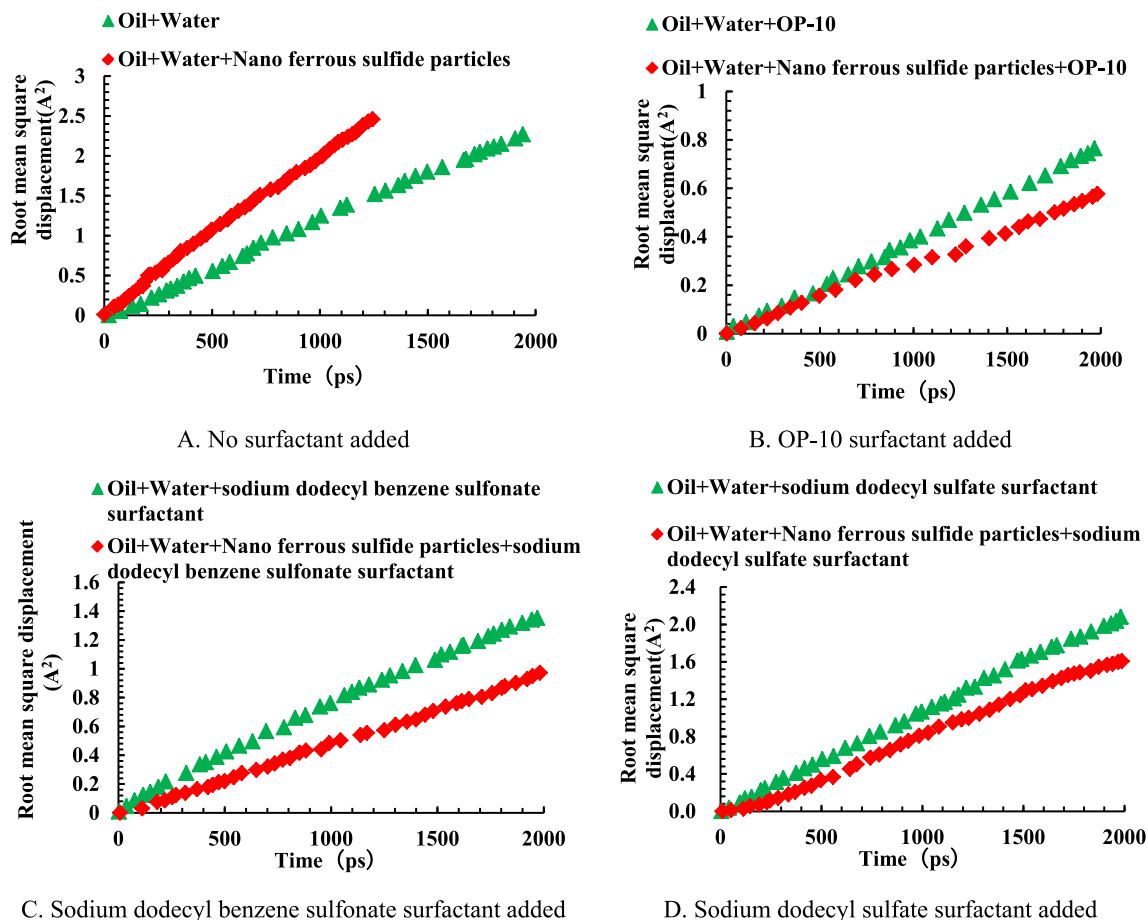


Fig. 11 Distribution of the root mean square displacement of water molecules under different conditions.

phases. These results show that the surfactant enhances the interfacial film strength so oil and water molecules maintain relatively stable. The influence of different surfactants on the distance between oil and water molecules was analyzed and the obtained results were compared with the experimental data. The comparisons are summarized in Table 6.

Table 6 indicates that there is a certain correspondence between the interfacial distance of oil and water molecules at the interfacial film and stable emulsion. The larger the distance between oil and water molecules, the stronger the stability of the emulsion, and the larger the maximum voltage which is applied to the emulsion system. These results indicate that surfactants can significantly enhance the stability of the emulsion. Fig. 11 shows the distribution of root mean square displacement

of water molecules against different surfactants and solid particles.

In this article, the root mean square displacement reflects random collisions between different molecules, which result in irregular motion of molecules. Therefore, it also reflects the diffusion coefficient. The slope of the curves in Fig. 11 represents the free movement ability of water molecules. It is observed that as the slope of the curve increases, the root mean square of displacement of water molecules increases, and the free movement of water molecules intensifies. Fig. 11 also shows that adding a certain amount of ferrous sulfide nanoparticles weakens the free movement of water molecules in the emulsifying system. This indicates that ferric sulfide nanoparticles can effectively adsorb water molecules and limit their free

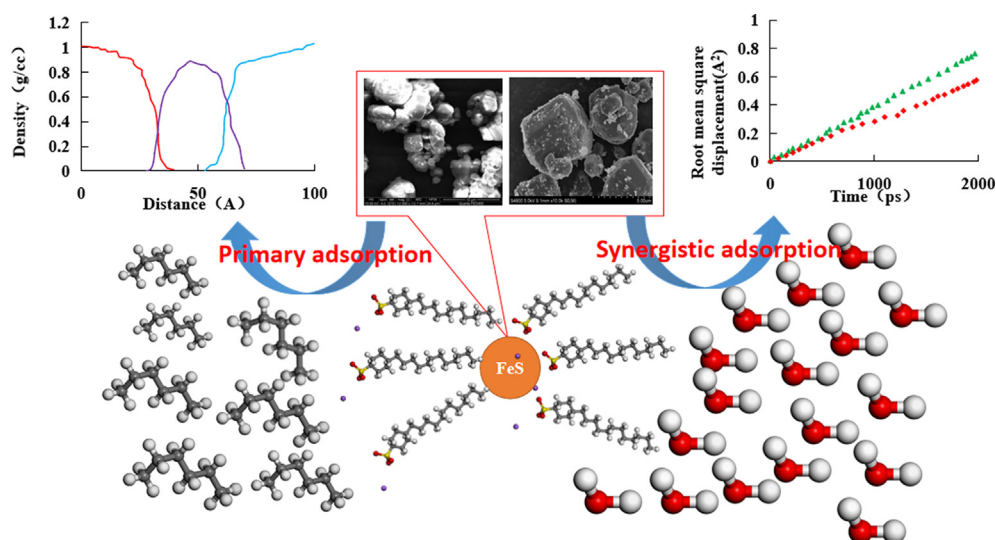


Fig. 12 Mechanism of the synergistic effect of surfactant and ferrous sulfide nanoparticles.

motion in the interfacial film, thereby increasing the strength of the interfacial film. The distributions of root mean square displacement of water molecules after adding different surfactants are shown in Fig. 11B, 11C, and 11D. Compared with Fig. 11A, the free movement of water molecules in the system was further limited by the synergistic effect of surfactant and ferrous sulfide nanoparticles. The root mean square displacement of water molecules decreased, which reinforced the interfacial film strength between oil and water molecules. The mechanism of strong emulsion stability in the produced fluid after acidizing ASP flooding under the synergistic effect of ferrous sulfide nanoparticles and surfactant was shown in Fig. 12.

The lipophilic and hydrophilic groups of surfactants affect the adsorption capacity of oil and water in the liquid film. Meanwhile, the free motion of oil and water molecules in the liquid film was restricted, thereby reinforcing the strength of the emulsion liquid film. However, the surfactant had a certain ability of free motion, which limits the free motion of molecules in the liquid film (Lu et al., 2022). When ferrous sulfide nanoparticles were added, the surfactant was adsorbed on the surface. Since ferrous sulfide nanoparticles have a relatively weak free motion, the ability of surfactants to control the oil and water phase strengthens under the synergistic effect of surfactant and ferrous sulfide nanoparticles (Dordzie and Dejam, 2021). It is concluded that when the surfactants and ferrous sulfide nanoparticles were added to the oil–water emulsion simultaneously, the liquid film strength of the emulsion further improves. In this case, stable emulsion forms and oil and water phases can be hardly separated.

4. Conclusion and discussion

After acidizing oil wells by alkali/surfactant/polymer (ASP) flooding, a strong stable emulsion system forms in the produced fluid. In order to analyze the generation of emulsion and the synergistic effect between liquid film under multiple factors, experimental data and simulation results were analyzed. The main conclusions can be summarized as follows:

- After acidizing by ASP flooding, solid particles in the intermediate layer were mainly ferrous sulfide nanoparticles.
- There were a large number of sulfate-reducing bacteria in the produced fluid after acidizing oil wells by ASP flooding, which could interact with the sulfate in the formation of water and produce hydrogen sulfide after metabolism. The produced hydrogen sulfide gas reacted with metal particles in the wellbore environment and ferrous sulfide particles are produced.
- The surfactants were adsorbed on the surface of ferrous sulfide nanoparticles. The nano-solid particles in the liquid film combined with the surfactant would further enhance the ability of the surfactant to control oil and water phases. The synergistic effect of nano-ferrous sulfide and surfactant significantly increased the strength of the interfacial film between oil and water.
- Although the generation of a strong emulsion system was analyzed in this work, the separation method was not studied in depth. It is intended to focus on multiple synergistic emulsifications of the strong stable emulsifying system in the next research. To this end, a high-strength centrifugal separation device will be set up to preferentially separate the solid particles in the emulsion system and break this emulsification balance.

Declaration of Competing Interest

The authors declare that they have no known competing financial interests or personal relationships that could have appeared to influence the work reported in this paper.

References

- An, H., Cao, G., Bai, Y., Wang, D., Meng, F., 2021. Study on the stability of emulsion based on molecular dynamics. *J. Dispers. Sci. Technol.* 42 (11), 1723–1732. <https://doi.org/10.1080/01932691.2021.1931290>.
- Bai, Y., Cao, Guangsheng, Nan, Xiaohan, Li, Shining, An, Hongxin, Wang, Xin, Wang, Zhe, 2021. Effect of sodium fluosilicate particles in acidification flowback fluid on emulsification stability of crude oil. *J. Petrol. Sci. Eng.* 202. <https://doi.org/10.1016/j.petrol.2021.108484>.

- Barg, S., Binks, B.P., Wang, H., Koch, D., Grathwohl, G., 2012. Cellular ceramics from emulsified suspensions of mixed particles. *J. Porous Mater.* 19 (5).
- Bin, H., Xiaohan, N., Cheng, F., et al, 2022. Probing the Coalescence Mechanism of Oil Droplets in Fluids Produced by Oil Wells and the Microscopic Interaction between Molecules in Oil Films. *Energies* 15.
- Cao, G., Bai, Yujie, Chen, Xiaolu, Nan, Xiaohan, Qingchao Cheng, Yu, Sui, Zhe Wang, 2021. Hydrate prevention based on convection and diffusion in alternate injection wells of carbon dioxide and water. *Case Stud. Thermal Eng.* 24. <https://doi.org/10.1016/j.csite.2021.100858>.
- Cao, G., Tong, Du, Bai, Yujie, 2021. Tingyuan Yang, Jize Zuo. Effects of surfactant molecular structure on the stability of water in oil emulsion. *J. Petrol. Sci. Eng.* 196, 107695. <https://doi.org/10.1016/j.petrol.2020.107695>.
- Cisneros-Dévara, R., Cerón-Camacho, R., Soto-Castruita, E., Pérez-Alvarez, M., Ramírez-Pérez, J.F., Oviedo-Roa, R., Servín-Nájera, A.G., Buenrostro-Gonzalez, E., Martínez- Magadán, J.M., Zamudio-Rivera, L.S., 2019. A theoretical study of crude oil emulsions stability due to supramolecular assemblies. *Coll. Surfaces A: Physicochem. Eng. Aspects* 567.
- Di, W., Xia, F., Sen, L., Xun, C., Huiping, Z., Wenjie, L., Yinghui, L., Rui, Z., Yuwei, Z., Xin, Z., Jianjun, Y., Nannan, G., 2021. Effects of secondary emulsification of ASP flooding produced fluid during surface processes on its oil/water separation performances. *J. Petrol. Sci. Eng.* 202. <https://doi.org/10.1016/j.petrol.2021.108426>.
- Dordzie, G., Dejam, M., 2021. Enhanced oil recovery from fractured carbonate reservoirs using nanoparticles with low salinity water and surfactant: A review on experimental and simulation studies. *Adv. Colloid Interface Sci.* 102449.
- Hong, J.Z., 2012. The Influence Fraction to the Crude Oil Emulsion Stability. *Adv. Mater. Res.* 1762 (502–502).
- Huang, B., Nan, X., Fu, C., Guo, T., 2021. Study of the bubble collapse mechanism and its influencing factors on stability under ultra-low surface tension. *Coll. Surf. A: Physicochem. Eng. Aspects* 618. <https://doi.org/10.1016/j.colsurfa.2021.126440>.
- Keliang, Wang, Bowen, Zhang, 2019. Li Gen. Effects of weak-alkali ASP composition on the stability of O/W emulsions. *Energy Sources, A: Recov. Util. Environ. Eff.* 41 (4), 1–13. <https://doi.org/10.1080/15567036.2018.1520328>.
- Li, D., Gao, B., Cui, X., 2022. Emulsifying behavior between oil and water of flowback fluids from acidizing oil wells based on high-voltage electric field oil–water separation technology. *New J. Chem.* <https://doi.org/10.1039/D2NJ02306G>.
- Li, S., Wang, F., Yang, Z., Xu, J., Liu, H., Zhang, L., Xu, W., 2020. Emulsifying performance of near-infrared light responsive poly-dopamine-based silica particles to control drug release. *Powder Technol.* 359.
- Lu, Z., Hu, Y., Zhang, B., et al, 2022. Anti-migration performance of EPDM composite improved by octadecylamine-functionalized graphene oxide. *J. Appl. Polymer Sci.* 139 (31), 52713.
- Mahdavi, S.Z., Aalaie, J., Miri, T., Razavi, S.M.R., Rahmani, M.R., 2017. Study of polyacrylamide-surfactant system on the water–oil interface properties and rheological properties for EOR. *Arab. J. Chem.* 10 (8), 1136–1146.
- Nishizawa, N., Kawamura, A., Kohri, M., Nakamura, Y., Fujii, S., Ngai, T., 2016. Polydopamine Particle as a Particulate Emulsifier. *Polymers* 8 (3).
- Qing, Z., Bai, R.-X., Guo, T., Meng, T., 2015. Switchable Pickering Emulsions Stabilized by Awakened TiO₂ Nanoparticle Emulsifiers Using UV/Dark Actuation. *ACS Appl. Mater. Interf.* 7 (33).
- Sharma, T., Kumar, G.S., Sangwai, J.S., 2015. Viscoelastic Properties of Oil-in-Water (o/w) Pickering Emulsion Stabilized by Surfactant-Polymer and Nanoparticle–Surfactant–Polymer Systems[J]. *Ind. Eng. Chem. Res.* 54 (5), 1576–1584.
- Sui, Xin, Chen, Zhao, Ivan Kurnia, Xu, Han, Jianjia Yu, Zhang, Guoyin, 2020. Alkaline - surfactant - polymer flooding of active oil under reservoir conditions. *Fuel* 262, 116647. <https://doi.org/10.1016/j.fuel.2019.116647>.
- Sun, C., Guo, H., Li, Y., Jiang, G., Ma, R., 2020. Alkali Effect on Alkali-Surfactant-Polymer (ASP) Flooding Enhanced Oil Recovery Performance: Two Large-Scale Field Tests Evidence Article ID 2829565 *J. Chem.* 2020, 22. <https://doi.org/10.1155/2020/2829565>.
- Taylor, S.E., Chu, H.T., 2018. Metal Ion Interactions with Crude Oil Components: Specificity of Ca²⁺ Binding to Naphthenic Acid at an Oil/Water Interface. *Colloids Interfaces* 2 (3), 40. <https://doi.org/10.3390/colloids2030040>.
- Wang, D., Cao, G., Bai, Y., Yang, X., Zhang, Z., 2020. Experimental study on the causes and critical conditions of toxic gases in hydraulically fractured oil wells. *Energy Sources, A: Recov. Util. Environ. Eff.* 42 (24), 2963–2971.
- Wang, J., Huang, Y., Zhou, F., Song, Z., Liang, X., 2020. Study on reservoir damage during acidizing for high-temperature and ultra-deep tight sandstone. *J. Petrol. Sci. Eng.* 191, 10723. <https://doi.org/10.1016/j.petrol.2020.107231>.
- Wei, W., Ting, W., Yi, C., Liu, J., Liu, X., 2015. Self-assembled micelles based on branched poly(styrene-alt-maleic anhydride) as particulate emulsifiers. *RSC Adv.* 5 (2).
- Zhang, Z., Cao, Guangsheng, Zuo, Jize, Bai, Yujie, 2020. Rheological properties and plugging behavior of active crude oil. *Petrol. Sci. Technol.* 38 (2), 131–145. <https://doi.org/10.1080/10916466.2019.1690508>.